INSTRUMENTS AND METHODS

A DIGITAL LOW-FREQUENCY, SURFACE-PROFILING ICE-RADAR SYSTEM

By David L. Wright,

(U.S. Geological Survey, M.S. 964, Box 25046, Federal Center, Denver, Colorado 80225, U.S.A.)

Steven M. Hodge,

(U.S. Geological Survey, University of Puget Sound, Tacoma, Washington 98416, U.S.A.)

Jerry A. Bradley, Thomas P. Grover,

(U.S. Geological Survey, M.S. 964, Box 25046, Federal Center, Denver, Colorado 80225, U.S.A.)

and Robert W. Jacobel

(Department of Physics, St. Olaf College, Northfield, Minnesota 55057, U.S.A.)

Abstract. A new short-pulse digital profiling radar system that operates at lower frequencies than most ice radars used in polar regions to date has been designed and built by the U.S. Geological Survey. The transmitter is an avalanche transistor pulser which drives a resistively loaded dipole transmitting antenna. A similar, but separate antenna is connected to the receiver. The receiver has adjustable sensitivity time control (STC) of as much as 60 dB to compensate for attenuation and geometric spreading factors. A fiber-optic cable is used to transmit both control signals and data. The data-acquisition and display system incorporates very high-speed digitizing and signal averaging, real-time profile display, and data storage on standard computer nine-track magnetic tape.

The system was successfully used on Ice Stream B in West Antarctica at centre frequencies of 1, 2, 4, 8, and 12.5 MHz. Bottom-return signal-to-noise ratios of more than 40 dB were obtained at 2 MHz through 800 m of ice. Convoluted internal surfaces not related to present bottom topography were resolved within the ice streams and anomalous strong reflections or "bright spots" were identified near the base of the ice. At present, there is no satisfactory glaciological explanation for either of these observations.

INTRODUCTION

Surface and airborne radar systems for studies of polar and temperate ice have been used for some time. A number of radar systems and the general subject of electromagnetic studies of ice are well described in Bogorodsky and others (1985). One of the most successful systems for airborne sounding of deep polar ice was built by the Technical University of Denmark and provides a benchmark against which other systems may be compared. In one mode, it transmits a selectable length pulse containing a number of cycles of a 60 MHz carrier frequency (Skou and Sondergaard, 1976). Alternatively, this radar can employ pulse expansion and compression by frequency sweeping (chirping).

Another type of radar system, called a short-pulse or impulse radar, has been developed that ideally radiates only a single cycle at a centre frequency determined by the length of resistively loaded dipole antennas. By centre frequency we mean the frequency of the peak of the power spectrum of the radiated pulse. Commercial systems of this type typically operate at centre frequencies between 80 MHz and 1 GHz and are well known in shallow-ground studies (Ulriksen, 1983). A variation on this type of radar (Watts and Wright, 1981), using much longer antennas and therefore lower frequencies, was developed for airborne profiling of temperate ice (where liquid water is present), but has applications to polar ice as well, particularly when it is important to preserve phase information in the recorded wave form or when electromagnetic losses in the ice increase substantially with frequency. The radar system described in this paper is of the low-frequency short-pulse type, but uses a number of enhancements made possible by recent advances in analog and digital electronics and electro-optics (Wright and others, 1989).

The system was used on Ice Stream B in West Antarctica during November and December 1987. The objective was to use radar on the ice stream to learn about its past and present behavior, its internal structure and basal conditions, and its possible response to climatic warming. The radar system was operated at 1, 2, 4, 8, 12.5 MHz and some lines were profiled at several frequencies to permit quantitative examination of trade-offs between parameters such as signal-to-noise (S/N) ratio and resolution. In addition, it is expected that a synthesis of the data recorded at different frequencies will yield more information about physical phenomena within the ice and at the bed.

SYSTEM DESCRIPTION

Electronic

A block diagram of the system is shown in Figure 1. The transmitter and receiver, shown within the dashed outlines, are both towed behind the instrumentation hut. The digital data-acquisition system (DAS), computer, tape drive, and gain-control unit are inside the hut and are powered by a 4 kW gasoline-powered generator. This system was designed specifically for acquisition, averaging, recording, and display of data in digital form while profiling, hence the DAS is central to the operation of the system. A digital oscilloscope could be substituted for the DAS, but with significant reductions in averaging and data-transfer rates. A full description of the DAS is given in Wright and others (1989).

The battery packs for the transmitter and receiver
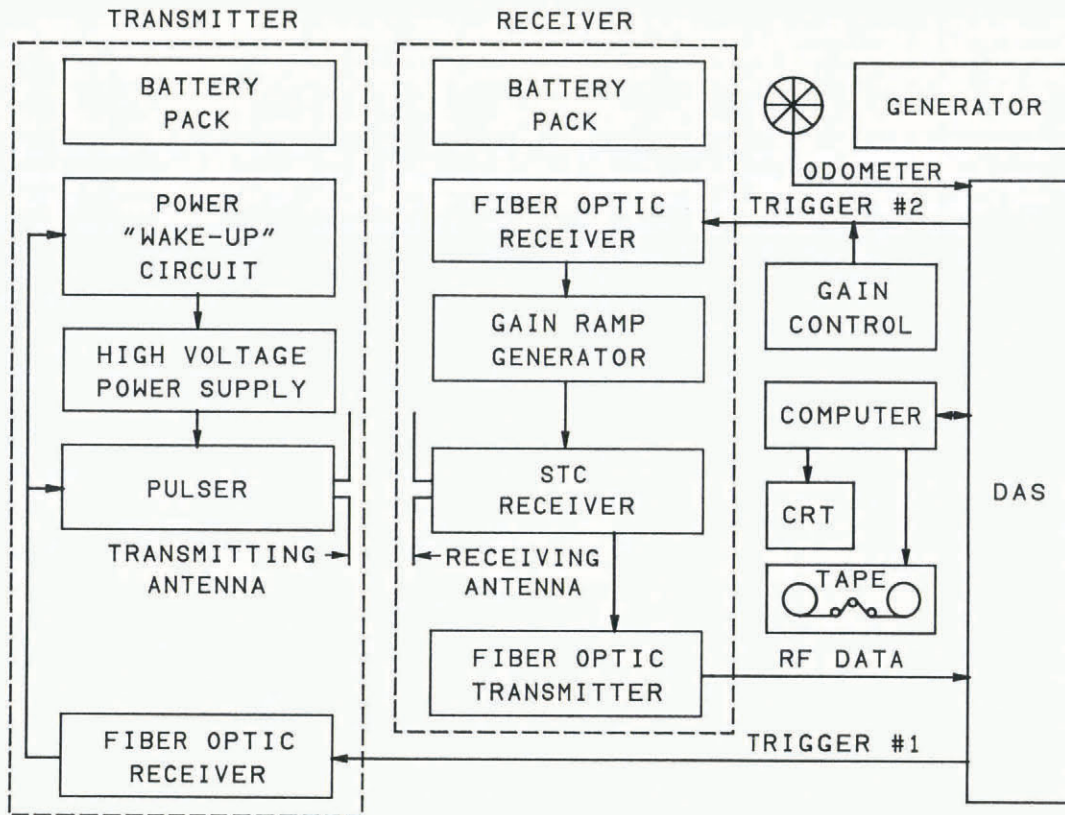
Fig. 1. *Block diagram of the electronics of the ice-radar system. Trigger #1 first turns on the latching "wake-up" circuit to apply high voltage to the pulser; subsequent trigger signals fire the pulser. Trigger #2 initiates the gain ramp in the receiver. Sensitivity time-control (STC) gain set-up commands are also transferred on this channel. All trigger signals and the radio-frequency analog data are transmitted over a multi-fiber-optical (F/O) cable.*

consist of six sealed lead–acid 6 V batteries rated at 8 A-h capacity. The current requirements for the transmitter depend on the transistor type used, since different types have different break-down voltage ratings, and on the repetition rate of the pulser. As operated in Antarctica, the transmitter required approximately 750 mA at 30 V at a repetition rate of 5 kHz. The battery capacity is sufficient for 8 h of non-stop operation under these conditions, even allowing for some derating of the batteries.

Because the high-voltage transmitter power supply consumes the most power, even when the pulser is not firing, a "wake-up" circuit is employed that applies voltage to the input terminals of the power supply only when trigger pulses are sensed. The trigger pulses are generated by the DAS. If the system is in stand-by mode (no pulses), the battery packs will last for more than 24 h.

The high-voltage power supply, a Venus Scientific Model F-6, has an output voltage adjustable over a range of 300–700 V and will maintain a constant output voltage over a range of input voltages from 24–31 V. The first feature allows different transistor types to be used in the pulser, and the second provides a constant transmitted signal level even though battery voltage decreases during operation.

Electromagnetic coupling between the transmitter, receiver, and vehicles was minimized by using a Siecor all-dielectric construction multi-fiber optical cable that carries trigger signals, control commands, and the radio-frequency received signal. Each of the lines passing through the dashed boxes in Figure 1 represents one fiber in the multi-fiber cable. The optical cable was also used as the tow cable for the transmitter and receiver.

The transmitter, shown in Figure 2, is a three-stage avalanche transistor Marx-bank pulser. A Marx-bank is a bank of capacitors charged in parallel, but discharged in series to gain a voltage multiplication. The transmitter is similar in many respects to the older model used for the airborne sounding of Columbia Glacier, Alaska (Watts and
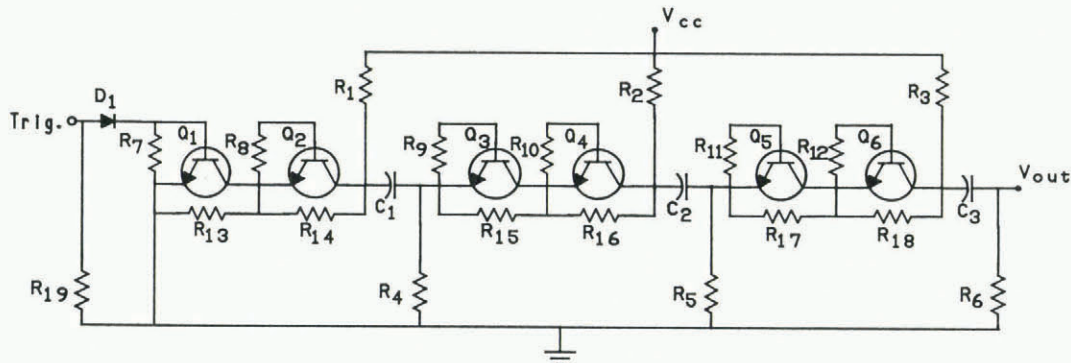
Fig. 2. *The three-stage avalanche-transistor pulser. This pulser can be built in a box of about 200 cm³ and weighs only about 200 g, yet delivers peak output power in excess of 10 kW at a repetition rate of up to 10 kHz. V_{cc} ranges from 300 to 600 V depending on the transistor type used. A TTL logic level is often adequate as a trigger. Further discussion and a parts list (Table I) are in the Appendix.*

Wright, 1981). Depending on the transistor type used in the new model, the peak power output may be slightly greater or less than that of the older pulser. Unlike the earlier version, the present one is triggered rather than free-running so that the transmitted pulses maintain phase coherence with the 100 MHz clock that controls DAS timing. The ability to trigger the transmitter synchronously with sub-nanosecond shot-to-shot jitter maximizes the benefits of digital wave-form addition, discussed later, and makes it possible to obtain uniform spatial data density in spite of vehicle speed variations. The pulser is compact, light, easy to build, and relatively reliable if certain construction and operational precautions are observed (see Appendix). Further discussion of avalanche transistor circuits is available in Herden (1976), Henebry (1961), and Nicholson and others (1976).

The receiver design presented some challenges because of limited dynamic range in the analogue optical link and the digitizer. Dynamic range for a linear analog system is the ratio of the maximum input signal for linear operation to the minimum detectable input signal. The dynamic range of a digitizer is approximately $6 \times n$ dB where n is the number of bits. A design criterion for the radar system was to use a very high-speed DAS with a 100 Megasample/s digitizer and high-speed wave-form addition for S/N enhancement (Wright and others, 1989). The digitizer, a LeCroy TR8818A, is an eight-bit device and thus provides only 48 dB of dynamic range. In addition, the fiber-optic link used to transmit the radio-frequency received signal to the digitizer has a dynamic range of only about 50 dB at the frequencies we are using. Much greater dynamic range is required to resolve important features present in the wave form, but whose return amplitudes are small compared to the surface and bottom returns, and to compensate for signal attenuation in the ice. For this reason, sensitivity time control (STC) was built into the receiver (Fig. 3).

STC, also known as time-varying gain, increases the sensitivity (gain) of the receiver as a function of time (proportional to distance) to compensate for the smaller amplitude of return signals from more distant objects. In a period as short as 2 µs, the gain can be smoothly varied by as much as 60 dB. The ability of the amplifier to present received signals, separated in time by as little as 2 µs and differing in amplitude by as much as 60 dB, to the digitizer at the same amplitude (though not with the same S/N ratio) compensates for the limited dynamic range of the digitizer and fiber-optic link. An electromechanical programmable attenuator precedes the receiver, but is used only when very large signals would saturate the amplifiers. In Antarctica, except for the lowest frequencies, no such attenuation was used so that the system could achieve the best S/N ratio. In this case, the pre-amplifier restricts the electronic linear dynamic range to about 60 dB although limited momentary overloads can be tolerated.

The wave-form averaging performed in the DAS improves the S/N ratio and effectively provides additional dynamic range subject to the restrictions discussed below. In Antarctica, we generally coherently added 4096 wave forms for a theoretical S/N improvement of 36 dB. The actual improvement was essentially equal to the theoretical improvement except for some slight system-generated coherent noise discussed below. When added to the 60 dB

electronic dynamic range, the system thus provided the equivalent of 96 dB, or 16 bits, of linear dynamic range without using the programmable attenuator.

The maximum number of wave forms that the DAS can add without overflow is 65 536 (2^{16}). Normalization is not used in order to preserve the full dynamic range. For uncorrelated Gaussian noise and a coherent (phase-preserving) receiver the theoretical S/N (power) enhancement derived from signal addition is $10 \times \log_{10}(n)$ where n is the number of wave forms added, thus the maximum enhancement by the DAS, apart from any separate computer addition which was not done in the field, but could be performed on the recorded data, is 48 dB. Coherent addition of wave forms, however, assumes that all signals add in phase; therefore, a limit is set on the physical distance that may be traveled while adding. The distance limit is a function of (a) the geometrical shape and roughness of "targets of interest", such as bottom topography, crevasses, or internal layers, (b) possible vertical antenna motion due to surface roughness (or aircraft motion in airborne applications), and (c) the wavelength of the radiated signal. The limit is more severe for higher frequencies (shorter wavelengths). A safe practice followed in bore-hole radar applications (Wright and others, 1986) is to restrict the motion of the transmitter and receiver to no more than one-tenth of a wavelength during addition. Such a stringent limit is not always necessary in ice, but in our Antarctic profiling the horizontal distance traversed during addition was generally about 1 m, thus this severe condition was satisfied even at the highest frequency used. Therefore, all return signals, including those from the smallest features detectable by the system, were added in phase during the entire addition process.

Another performance figure, sometimes confused with receiver dynamic range, is "system sensitivity" which is sometimes given as the ratio of the transmitter maximum output power to the receiver minimum detectable signal. We refer to this ratio as the "electronic" system sensitivity. Additional factors, including antenna gain, system losses such as those due to antenna and cable resistivity, pulse expansion and compression, if any, and signal recording enhancements need to be included when making *total* system sensitivity comparisons. For the system described here the minimum detectable signal power, with no additional signal processing, is theoretically −90 dB m (10^{-12} W). The peak output power from the pulser is +70 dB m (10^4 W), so the theoretical electronic system sensitivity is 160 dB. Laboratory measurements show an electronic system sensitivity of about 145 dB. The 15 dB reduction is due to television and radio transmissions in the pass band of the receiver, and to some system-generated digital noise from the gain-control circuitry. Since there is very little television and radio interference in Antarctica, the system sensitivity should be somewhere between these two values. Careful noise measurements were not made in the field because the calibrated oscillator used for signal level measurements was not available.

For our system, the antennas are resistively loaded to shape the radiated pulse and are less directional than those of higher-frequency multi-element antennas. Although measurements on our antennas are not available, theoretical calculations place the (two-way) net antenna directional gain
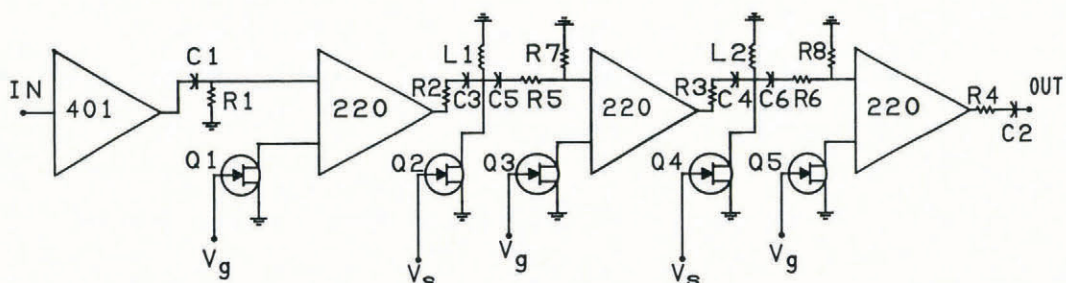
Fig. 3. The receiver–amplifier circuit diagram. Sensitivity time control was accomplished using a three-stage cascade of wide band-width operational amplifiers with the gain set by low-capacitance field-effect transistors (FETs) used as voltage-controlled resistors. A parts list is in Table II in the Appendix.

plus resistive losses in the range of −2 to −16 dB, depending on antenna loading. Adding the antenna loss and the 36 dB gain from wave-form addition to the electronic system sensitivity gives a total system sensitivity of 165−179 dB using the laboratory measured receiver-noise figure, or 180−194 dB if the receiver reached its theoretical noise limit. If the DAS were allowed to add to its full capacity, a total system sensitivity of 192−206 dB is theoretically possible, but this may be impractical, except for very local studies, because of the phase coherence requirement.

For comparison, the 60 MHz tuned radar system developed by the Technical University of Denmark (TUD) has a maximum transmitter power of 10 kW, the same as our radar system, but has an electronic system sensitivity, depending on selected band width, of 171−182 dB (Skou and Sondergaard, 1976). Antenna gain, system losses, and recording gain must be added to arrive at the total system sensitivity. Skou and Sondergaard calculated a 22 dB two-way antenna gain, including a small antenna feed-system loss, and estimated a photographic recording gain of 15 dB at typical airborne recording speeds. These additions, less a small loss in the transmit/receive switch, give a total system sensitivity for the TUD system of 207−218 dB. If used on the ice surface with fast digital signal addition such as that provided by our DAS, even higher total system sensitivities might be possible. Our DAS has already been successfully used with the TUD radar system in airborne profiling of the Greenland ice sheet (Wright and others, 1989).

Estimates of range versus system sensitivity can be derived from the "radar equation" which is discussed in many radar texts such as the one by Skolnik (1962). This equation, specialized to the case of reflection from a planar interface, may be written in the form

$$\frac{P_r}{P_t} = \frac{(G\eta\lambda\rho)^2}{4(4\pi)^2} \frac{e^{-4\alpha R}}{R^2}$$

where P_r is the received power, P_t is the transmitter power, G is the antenna gain where we assume that the transmitting and receiving antennas are identical, η is the antenna and feed-system efficiency, λ is the wavelength in meters, ρ is the electric field reflection coefficient at the ice−rock interface, given by

$$\rho = \frac{(\varepsilon_r)^{\frac{1}{2}} - (\varepsilon_i)^{\frac{1}{2}}}{(\varepsilon_r)^{\frac{1}{2}} + (\varepsilon_i)^{\frac{1}{2}}}$$

for normal incidence where ε_r and ε_i are the relative dielectric permittivities of rock and ice, respectively. R is the distance in meters measured from the transmitting antenna to the bottom. We ignore the fact that the receiving antenna is not at the same location as the transmitting antenna because, for separation distances small compared to the ice thickness, the correction does not substantially alter the results. α has the units of m^{-1}, and is related to the effective attenuation in dB/m by the relation

$$A(dB/m) = 8.686\alpha.$$

The effective attenuation excludes the geometric spreading factor, R^{-2}, but includes all other means by which power density is reduced in the propagating wave, including conductive losses in the ice which convert electromagnetic energy to heat, scattering and diffraction from inhomogeneous inclusions and crevasses in the ice, and specular reflection from interior ice surfaces. An example is plotted in Figure 4 with effective attenuation in dB/m as a parameter. To generate these curves, we assume that G is 1.6 which is appropriate for a half-wave dipole in free-space and is an underestimate when the antenna lies on the air−ice interface. The antenna efficiency is taken to be 10%, the wavelength is taken to be 84 m which corresponds to a frequency of 2 MHz in ice if the ice has a relative permittivity of 3.2, and the relative permittivity of the rock underlying the ice is taken to be 10, giving a reflection coefficient of 0.277. The −150 dB level in Figure 4 represents the estimated detection limit set by the electronic sensitivity of our system with no wave-form addition.
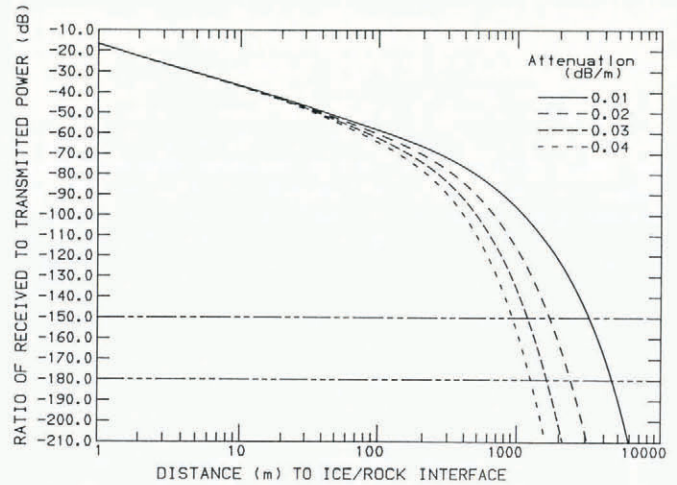
Fig. 4. *The ratio of received to transmitted power for our system, when operated at a centre frequency of 2 MHz, versus distance to the ice−rock interface with effective attenuation as a parameter. For short distances, the curves are dominated by the geometrical spreading (R^{-2}) factor. For large distances, the curves are dominated by the attenuation $(e^{-4\alpha R})$ factor. The left-hand intercept is at −16 dB, partly because of the assumed antenna efficiency of 10%.*

During static tests on Ice Stream B we noted a bottom-return S/N ratio of slightly more than 40 dB at 2 MHz through 800 m of ice when adding 4096 wave forms (36 dB of enhancement). This indicated that the bottom return should have been detectable under these conditions with no wave-form addition. Indeed, this was the case. Comparing this result to the curves in Figure 4, we estimate that the effective attenuation in the ice may have been as much as 40 dB/km. For this effective attenuation, and with the system parameters we assumed above, the range limit with no wave-form addition is about 900 m, and with 36 dB of S/N enhancement the range limit is about 1300 m. If the effective attenuation were 30 dB/km in the ice, the range limits would be 1200 m with no wave-form addition and 1750 m with 36 dB of S/N enhancement and the same system parameters. For very cold ice, much greater ranges are possible. Estimates of expected attenuation versus ice temperature may be derived from data in Bogorodsky and others (1985). Since range clearly depends not only on system parameters but on the effective ice attenuation, which varies with ice temperature and factors such as crevassing and internal reflecting surfaces, a range obtained in a given field situation does not assure equal performance elsewhere. The older Watts and Wright (1981) system performance with identical field conditions and antennas would roughly equal that of our new system with no wave-form addition.

For sounding deep polar ice, the system with the highest possible system sensitivity is normally the system of choice. There are situations, however, where a lower frequency short-pulse system has advantages despite a lower system sensitivity. First, the short-pulse system is a coherent system and phase information is preserved. The TUD receiver and other gated carrier receivers usually, though not necessarily, use square-law detection and thus lose phase information. Preservation of phase information makes it possible, for example, to determine from a reflection at an interface between materials of differing dielectric permittivities which material has the higher permittivity. Secondly, wave-form addition improves the S/N ratio faster for coherent signals than for detected ones. Thirdly, conductivity and scattering losses often increase substantially with frequency in warm and crevassed ice, respectively. These losses are sometimes so great that a low-frequency system can have greater depth penetrating ability than higher-frequency radars with more sensitivity. Fourthly, operation at various frequencies within the wide pass band of the receiver is simply a matter of changing four wires that make up the antennas, whereas frequency changes for a tuned system are more complicated. Finally, the transmitter

and receiver for the short-pulse system are quite compact and light and can easily be battery powered, not usually the case for high-power tuned radar systems.

Resolution is another criterion by which radar systems are sometimes compared, where resolution is defined as the ability to distinguish two nearby objects from one another (not range accuracy or a limit on minimum detectable size). Details of radar resolution depend on factors such as radiated pulse shape, pulse length, and receiver characteristics, but in general a spatial separation corresponding to a two-way propagation time equal to or greater than roughly half the pulse length is required to resolve two objects. An ideal short-pulse system that radiates only one cycle of a sine wave of a given frequency would have a pulse duration equal to the cycle length, thus providing the best resolution possible at that frequency. The radiated wave form for our system is dependent on the resistive loading and length of the antennas. The antennas used on Ice Stream B were slightly underdamped, causing an additional "tail" of about 1 cycle which degraded the resolution. However, ignoring this tail, the ideal resolutions for our system are approximately 84, 42, 21, 10, and 7 m in ice at 1, 2, 4, 8, and 12.5 MHz respectively. For the TUD system, the pulse lengths can range from 1000 to 60 ns, yielding resolutions of about 80–5 m. The most common pulse length used with the TUD system is 250 ns, corresponding to about a 20 m resolution. Thus, except for degradation caused by pulse tails resulting from underdamped antennas in our system, the two radars yield similar resolutions.

In our system, a multi-fiber optical cable carried trigger signals, control signals, and data between the transmitter, the receiver, and the DAS. Digitally encoded control signals were sent over one fiber to the receiver to set the attenuator level, the base gain level, the gains in each of 15 time windows, the total length of the gain ramp, and the delay to the start of the ramp. The encoded gain settings were stored in a memory in the receiver and then, at each trigger signal, sequentially read out to a digital-to-analog converter which generated the voltages to be applied to the gain control and voltage-divider inputs on the receiver. Filtering was used so that the voltages changed smoothly from one time window to the next. The control unit also sent all the settings to the computer over a serial (RS-232C) port; these settings were recorded with the data on tape so that, if needed, a calibration correction can be applied to the data whenever relative signal amplitudes are important in interpretation.

An IBM PC/AT computer was used for a system controller. This computer set DAS parameters, read data from the DAS, read the odometer and the receiver control unit settings, displayed the data on a colour-graphics screen, and then wrote the data to a nine-track tape drive. Data were buffered into 6 Megabytes of extended memory while traversing along the surface, and dumped to the tape drive after coming to a complete stop. This avoided any potential problems which might be caused by actually writing to the tape drive during the occasionally rough ride over the snow surface. Several kilometers of profiling could be accumulated in this memory buffer. All software was written in assembly language, both for maximum speed and to make possible many of the required hardware tasks. Data were displayed in real time on a 256 colour, high-resolution (640 × 480 pixel) monitor.

Mechanical and thermal

The transmitter and receiver were placed in separate cylindrical tubes with conical ends so that they would ride over the wind-induced roughness (sastrugi) on the surface (Fig. 5). To ensure that the cylinders would not roll over, lead plates were placed in the bottom of each cylinder. The inside of each cylinder was lined with foam to provide both shock and thermal insulation. The cylinders were towed using the fiber-optic cable, which had Kevlar and fiberglass/epoxy stress members embedded in it.

The instrumentation hut, also shown in Figure 5, pulled the fiber-optic cable and was itself towed by a tracked vehicle. The hut was insulated both electromagnetically and thermally, and housed the control electronics, monitor oscilloscope, data-acquisition system, computer, and tape drive, as well as one or two operators. Power was supplied by a 4 kW gasoline-powered generator. The hut was carried

Fig. 5. The instrumentation hut, towing vehicle, and receiver. Sixteen low-pressure tires smoothed the ride over the sastrugi. The electric generator and odometer wheel (raised) are mounted on the rear platform. The radar receiver is in the cylinder in the left foreground. The fiber-optic cable was the tow cable for the transmitter and receiver, and the antennas were tied to this cable.

on an aluminum frame suspended by 16 low-pressure "all-terrain-vehicle" tires. These tires eliminated most shock and high-frequency vibration, and provided an undulating ride over the sastrugi. A heavy-duty bicycle wheel drove a shaft encoder to provide distance and speed information, and to achieve a uniform spatial data density by controlling the transmitter repetition rate.

During operation, the instrumentation, operators, and solar radiation supplied more than enough heat in the hut. After sitting for several hours with no power, the interior temperature of the hut would typically be in the 5–10 °C range depending on ambient temperature, wind, and cloud cover. At the beginning of each day's operations, a 1500 W electric heater and the tape drive were turned on to bring the hut interior temperature up to a minimum of 13 °C which was required before the tape drive would load a tape. The heater usually was needed for only 30–45 min. All of the other equipment could be started cold, although the usual practice was to allow the computer to warm prior to applying power. The interior temperature in the transmitter and receiver housings would often fall to −5 °C after sitting for several hours without any power, but power could be applied to both transmitter and receiver at this temperature without causing any problems.

FIELD EXPERIENCE

The radar system was used on the down-stream part of Ice Stream B, West Antarctica (Fig. 6) in November and December 1987 and proved highly successful in revealing bed and internal features in 800 m thick ice. Most of a 36 km longitudinal line and a 4 km transverse line were profiled at frequencies of 1, 2, 4, 8, and 12.5 MHz. Static tests were run at 2, 4, 8, and 12.5 MHz to determine the S/N ratio of the bottom echo. The S/N ratio at 2 MHz was in excess of 40 dB and diminished by roughly 10 dB per frequency doubling.

The system had a number of initial difficulties, but most of them were satisfactorily solved during our field work. A few characteristics of the system, however, require some minor redesign. The fiber-optic cable terminations were too fragile and will be strengthened by installing "break-out kits" to provide individual fibers with Kevlar strain relief. In all other aspects, the fiber-optic cable was very successful; it remained sufficiently flexible in the cold and was strong enough for use as a tow cable.

Some fluctuations in receiver output occurred, whose origin is not yet understood, but these fluctuations were not of sufficient magnitude to justify halting field operations to identify and eliminate the source. In addition, there was some leakage of gain-control digital switching noise into the signal path despite considerable efforts to filter and shield against such leakage. The noise is easily recognized and can
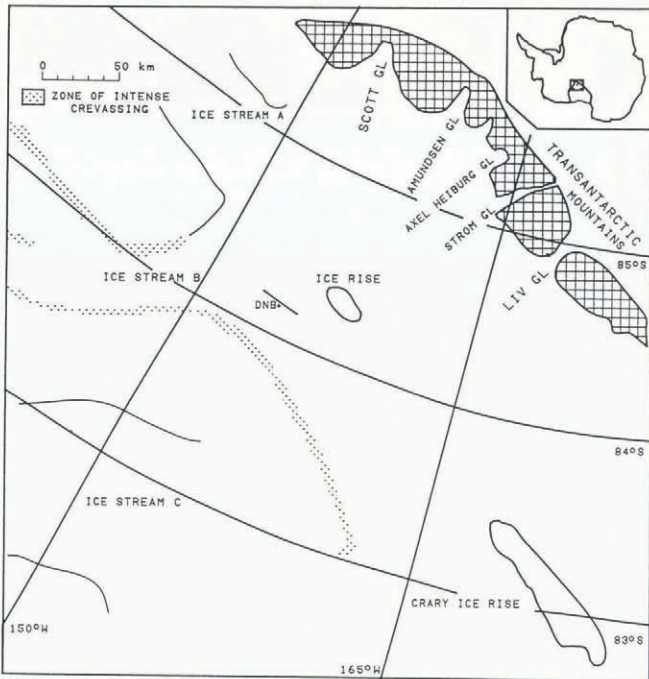
Fig. 6. Location map modified from Bindschadler and others (1987). The locations of the mouths of Ice Streams A, B, and C are shown. Also shown are the locations of the camp "Down-stream B" (DNB) and the adjacent line along which many of the profiles shown in the following figures were run. The line is locally parallel to the flow line of Ice Stream B.

Fig. 7. An 18 km long profile at 2 MHz. Along this profile, run along the line shown in Figure 6, there is convoluted internal structure that bears no resemblance to the nearly flat bottom topography.

be removed by digital processing. However, we plan to eliminate it by redesigning the gain-control circuit and by improved electromagnetic shielding.

FIELD RESULTS

A primary purpose of the 1987 field-season measurements described here was system development and testing. Nevertheless, the system performed well enough that about one Gigabyte of data was obtained. The data will take some time to analyze rigorously, but even without such analysis, simple play-back of the raw data, as illustrated in Figures 7–12, reveals several interesting and as yet unexplained features including prominent reflections from surfaces within the ice sheet which do not conform to the bottom topography.

An example is shown in Figure 7, which is an 18 km long, 800 m thick section parallel to the flow line of Ice Stream B. The horizontal dimension represents distance along the profile while the vertical dimension corresponds to time which we have converted to ice depth by assuming an average propagation velocity of 1.68×10^8 m/s in the ice. The top mark on the vertical axis indicates the arrival of the direct wave from the transmitter to the receiver. The lower mark indicates the arrival of the reflection from the bottom. Both the direct wave and the bottom reflection appear as bands rather than sharp lines because of the non-zero width of the radiated and reflected wave forms, discussed later, and because of the way signal amplitude is mapped into a colour scale reproduced here as a gray scale. The horizontal dimension is compressed by displaying only every thirty-sixth wave form, and the vertical dimension is compressed by displaying every second point in each displayed wave form. The centre frequency of the radar pulse was 2 MHz. Some constant horizontal lines were produced in this and succeeding figures by noise from the receiver gain-control circuit. These system artifacts can be removed by digital filtering.

Perhaps the most interesting features are prominent reflections from surfaces within the ice sheet which are unrelated to the present bottom topography. This is in marked contrast to internal layers seen in many places
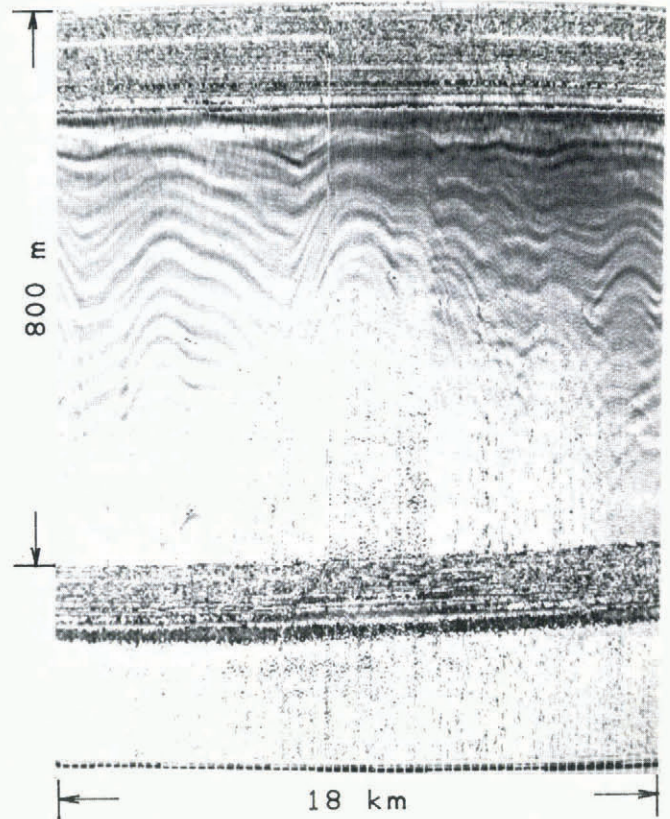
whose shapes are attenuated images of the bottom topography (Gudmandsen, 1975). Internal reflections are seen at all frequencies and on all profiles, but are stronger at lower frequencies because of the better S/N ratio. There are other examples where the vertical amplitude of internal layers exceeds that of the underlying basal topography and theory indicates that basal boundary conditions such as longitudinal variations in basal sliding and shear stress can lead to distortions of internal layers even without any bottom topographic variations (Whillans and Johnsen, 1983), but the character and very large amplitude of the internal surfaces observed in Ice Stream B may indicate that an alternative explanation is necessary (personal communication from R. Alley, 1988).

Figure 8 is another, mostly overlapping, section along the same profile, but the centre frequency in this case was 4 MHz. The shapes of the major internal features in this section are like those in Figure 7 although the resolution is better, lending confidence that the apparent internal structure is real and not a system artifact. Some of the apparent "double layering" in Figures 7 and 8 may be due to antenna ringing of about one extra cycle. Some of the deeper apparent layers in Figures 7 and 8 may also be multiples (second round trips) from shallower reflectors. Multiples, similar to bottom reverberations in marine seismic data, are infrequently observed in radar data, but examples can be seen in Narod and others (1988) and a very clear example is shown in Wright and others (1984). Pulse-compression techniques can be applied to the data to eliminate the double-layer effect, and algorithms exist for treating reverberations, but it is clear that several prominent reflecting surfaces would still remain. These surfaces rise and fall in smooth patterns covering many kilometers horizontally, and substantial fractions of the ice thickness vertically, and are clearly unrelated to the bottom topography, which is extremely smooth along the entire profile. We have chosen to refer to these patterns as internal "surfaces" rather than "layers", to emphasize that they do not conform to the bottom or surface topography, or, in many cases, to each other.
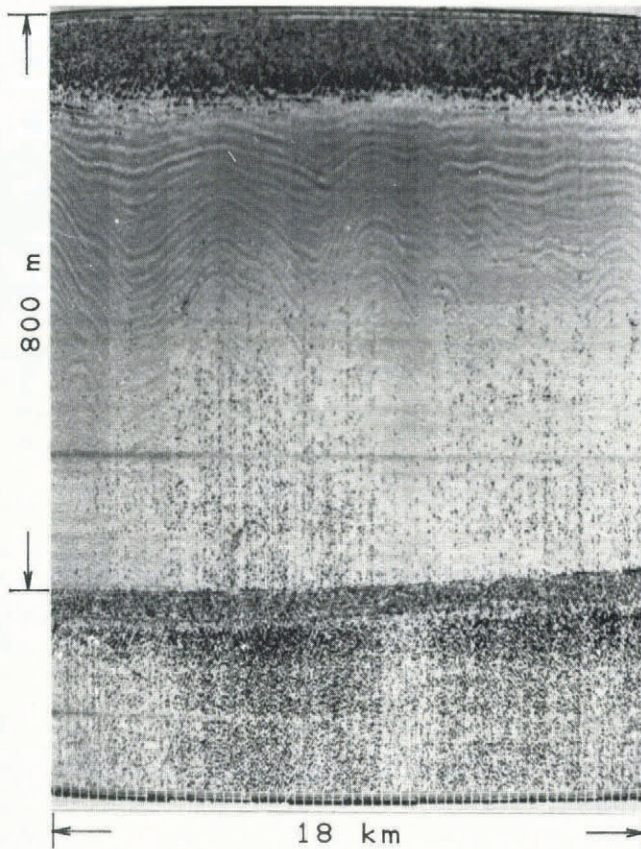
Fig. 8. An 18 km long profile at 4 MHz. This profile
largely overlaps the profile in Figure 7. Although the
resolution is higher and some reflections are weaker, the
shapes of the internal structures match those of the
previous figure as they should.

Fig. 9. A 4 km long transverse profile at 2 MHz. This
profile, perpendicular to the ice flow, shows that the
internal structure transverse to the flow appears generally
similar in character to that along the flow and much
broader than the diffraction patterns, faintly visible near
the surface and bottom, produced by crevasses. The
intersection of this profile with the longitudinal "Z" line is
indicated by the arrow.

These surfaces are evidence for complex and variable
ice flow. They could have been produced up-stream by
some unknown mechanism and transported into the area of
the measurements. One suggestion is that the surfaces we
observe might be due to "islands" or "rafts" of ice that have
been torn from inland ice up-stream and incorporated into
the ice stream (Shabtaie and others, 1987; Whillans and
others, 1987).

Another explanation has been considered that the
internal surfaces are buried zones of intense crevassing
produced during earlier active phases of the ice stream. If
one supposes that these zones are long curvilinear strings of
crevasses, often observed now at places on the surface, then
the apparent up and down trends of the surfaces could
result from these crevasses varying in distance horizontally
from the straight line of the measurement traverse. If so,
these measurements might yield information about the
number and timing of ice-stream active phases. However, if
this hypothesis is correct the buried crevasses must be
metamorphosed into smooth surfaces, because no chaotic
diffraction patterns characteristic of crevasses are in
evidence from these surfaces, although diffraction patterns
are seen near the air–ice surface and ice bottom as
discussed below.

As a further test of this hypothesis, profiles transverse
to the ice flow were run. An example is shown in Figure
9, in which the character of the surfaces is very similar to
that of the longitudinal profiles, running for hundreds of
meters, and the internal structure again does not show
diffraction hyperbolae produced by objects with sharp edges
as near-surface and bottom crevasses have. It therefore does
not appear that the surfaces are buried zones of crevasses.

It has also been suggested that the convoluted internal
surfaces may be due to historical velocity changes in the
ice flow of Ice Stream B. If the down-stream part of Ice
Stream B stopped for some reason while the up-stream part
was still moving, it might be imagined that ice would be
deformed.

It may be that none of the suggested explanations is
correct. The cause of the convoluted internal surfaces is an
open question.

Figure 10 shows an individual wave form (actually the
average of 4096 wave forms) displayed in "A-scope" fashion
with the wave amplitude represented by vertical displace-
ment rather than the colour scale used in the profile
displays or the gray scale of the photographic reproductions
shown in this paper. Because of the STC and the use of
separate transmitting and receiving antennas, no blanking
intervals are necessary and none is used in the receiver.
The first large pulse is the direct wave that propagates
along the air–ice interface from the transmitter to the
receiver; the second pulse is the bottom return. The small
"wiggles" between the direct wave and the bottom return are
due to inhomogeneities internal to the ice as seen in the
profiles. In order to calculate an accurate ice thickness
based on the time interval between the initiation of the
direct wave and that of the bottom return, it is necessary
not only to consider the speed of electromagnetic
propagation in the ice and a firn correction to that speed
but also to account for the 146.6 m separation between the
centers of the transmitting and receiving antennas. The
bottom return is almost as great in amplitude as the direct
wave, a consequence of the STC in the receiver. The
bottom-return wave form, although fairly compact, is not a
single cycle of a sine wave as would be radiated by an
ideally loaded and driven antenna. The additional cycle on
the wave form may indicate that the resistive damping on
this set of antennas was somewhat less than optimum, or
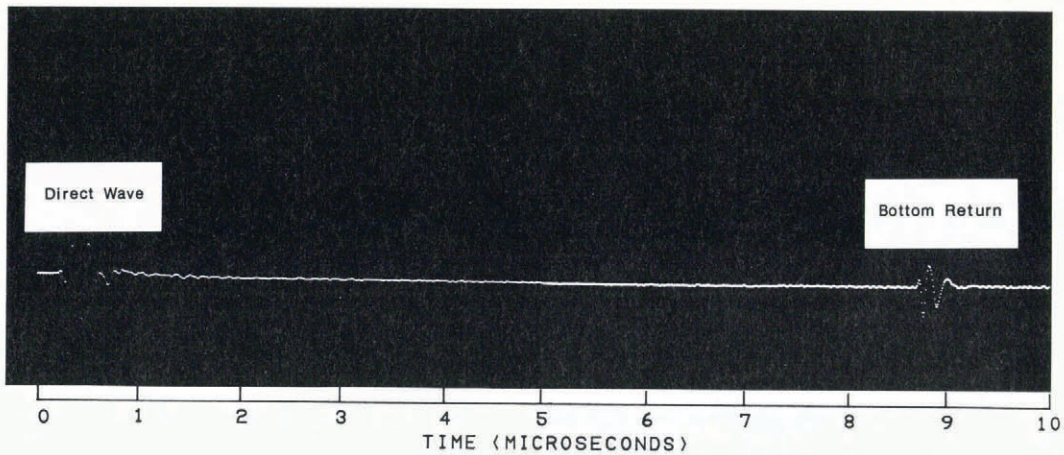
Fig. 10. An averaged wave form in "A-scope" style. The receiver sensitivity time control was adjusted so that the direct wave and bottom return are of similar amplitude. The much smaller "wiggles" in the wave form are generated by internal reflections in the ice.

that the bottom structure is more complicated than a single well-defined interface between ice and rock, or both. The direct wave form is, unfortunately, not representative of the wave form radiated into the body of the ice for two reasons: first, the wave form radiated by a loaded antenna driven by a pulse is not the same for broadside and axial directions (Wright and Prewitt, 1975); secondly, the received direct wave form is altered because the antennas lie on the air−ice interface. The bottom return may closely match the radiated wave form, but could be altered by dispersion in the ice or by a layered bottom structure. The non-zero duration of the direct and bottom wave forms causes the non-zero width direct and bottom return bands on the profiles. Full data analysis, including multiple-frequency comparisons will hopefully allow us to derive information about the bottom conditions. The recorded wave form will allow digital wave-form compression (deconvolution) similar to that done on airborne Columbia Glacier ice-radar data (Watts and Wright, 1981; Wright and others, in press).

Figure 11 shows a segment of the 4 MHz profile shown in Figure 8, but with only a four-fold compression in the horizontal dimension and no compression in the vertical dimension. The shallow fine structure is generated by diffraction from near-surface crevasses. Our system was not optimized to look at near-surface features, so the apices of the hyperbolae are masked by the non-zero duration of the direct wave from the transmitter. However, both higher-frequency radar and drilling confirmed the presence of near-surface crevasses. It is this kind of signature that one would expect to see if our internal surfaces were buried crevasses.

Figure 12 shows returns that appear both above and below the bottom level. Most of the returns that appear below the bottom are probably diffraction hyperbolae from bottom crevasses, but in some cases we may be observing small "bumps" in the bottom or possibly variations in a saturated till layer (Blankenship and others, 1987). There are also very strong reflections from features some distance above the bottom. One of them is a "bright spot", perhaps indicating the presence of free water, or bottom material carried by the ice.

Many interesting features such as these exist in our records. Digital processing and interpretation of substantial parts of the data will be time-consuming. Two processes that will be applied first are filtering to remove system-generated artifacts from the data and wave-form compression (deconvolution) to improve the resolution. A synthesis of data obtained at different frequencies will also be made to aid analysis of bottom conditions and internal structure. In addition, migration, a process by which geometrical factors are taken into account to move surfaces from their apparent positions into corrected positions, may be usefully employed on some of the data. Finally, reverberation removal can also be carried out. Careful processing and analysis of the data, including correlation with other relevant geophysical data, should enable us to contribute to the understanding of ice-stream dynamics.

CONCLUSIONS

The new surface-profiling ice radar using fiber optics and very fast digital signal averaging, recording, and real-time profile display has proven to be a very effective system. A few details need some improvement, but overall the system has exceeded our expectations in its ability to achieve good signal-to-noise levels. Not only are the bottom returns strong at Ice Stream B but convoluted internal surfaces have been revealed within the ice stream and anomalous bright spots were discovered near its base. These phenomena lack satisfactory explanations and should challenge the glaciological community to provide hypotheses that can explain them. Our results confirm our supposition
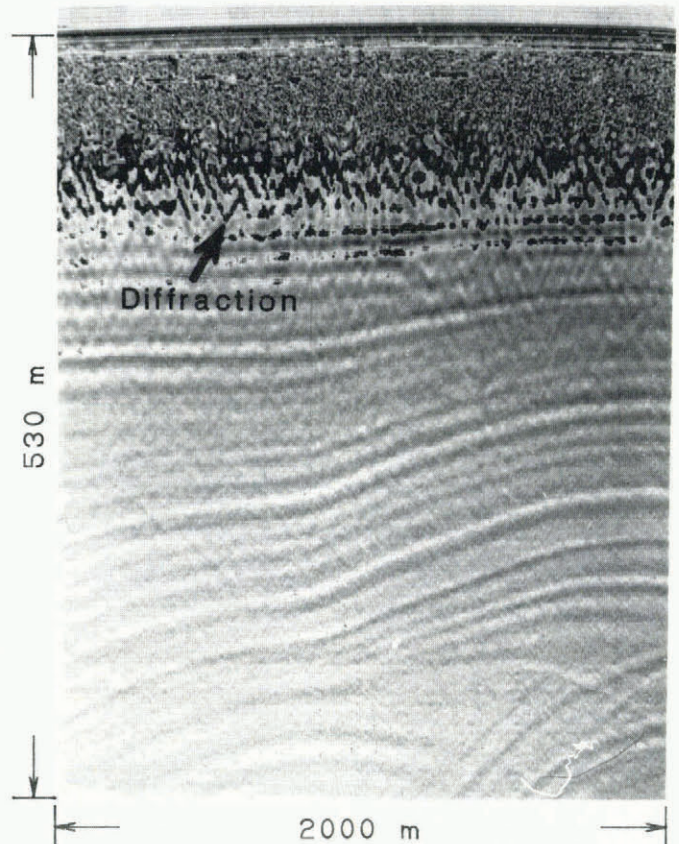
Fig. 11. A 2000 m long profile segment at 4 MHz. This example is from the same profile as Figure 7, but displayed at full vertical scale. The diagonal lines marked near the top are diffraction returns from near-surface crevasses.
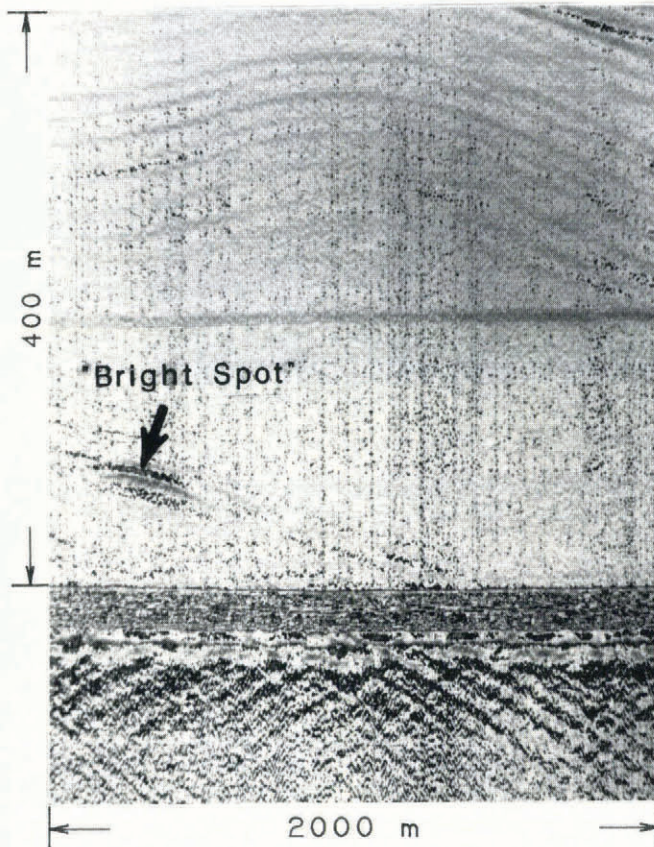
Fig. 12. A 2000 m long bottom profile segment at 4 MHz. This example is at full vertical scale and shows only the lower part of the ice and the bottom where strong diffraction patterns are generated. Careful analysis may indicate that some sub-bottom structure is also revealed. In addition, internal reflections are seen above the bottom return. One of these appears to be unusually intense and may indicate water or bottom material embedded in the ice.

that the use of short-pulse radar at frequencies lower than heretofore used on ice sheets can indeed yield new or complementary information to that obtained by higher-frequency radars. We are optimistic that the system can prove effective in further field studies on Ice Stream C in Antarctica, and other locations.

ACKNOWLEDGEMENTS

REFERENCES

Bindschadler, R.A., S.N. Stephenson, D.R. MacAyeal, and S. Shabtaie. 1987. Ice dynamics at the mouth of Ice Stream B, Antarctica. *J. Geophys. Res.*, **92**(B9), 8885-8894.

Blankenship, D.D., C.R. Bentley, S.T. Rooney, and R. Alley. 1987. Till beneath Ice Stream B. 1. Properties derived from seismic travel times. *J. Geophys. Res.*, **92**(B9), 8903-8911.

Bogorodsky, V.V., C.R. Bentley, and P.E. Gudmandsen. 1985. *Radioglaciology*. Dordrecht, etc., D. Reidel Publishing Company.

Gudmandsen, P. 1975. Layer echoes in polar ice sheets. *J. Glaciol.*, **15**(73), 95-101.

Henebry, W.M. 1961. Avalanche transistor circuits. *Rev. Sci. Instrum.*, **32**(11), 1198-1203.

Herden, W.B. 1976. Application of avalanche transistors to circuits with a long mean time to failure. *IEEE Trans. Instrum. Meas.*, **25**(2), 152-160.

Narod, B.B., G.K.C. Clarke, and B.T. Prager. 1988. Airborne UHF radar sounding of glaciers and ice shelves, northern Ellesmere Island, Arctic Canada. *Can. J. Earth Sci.*, **25**(1), 95-105.

Nicolson, A.M., H.M. Cronson, and P.G. Mitchell. 1976. Subnanosecond risetime pulse generators. *IEEE Trans. Instrum. Meas.*, **25**(2), 104-107.

Shabtaie, S., I.M. Whillans, and C.R. Bentley. 1987. The morphology of Ice Streams A, B, and C, West Antarctica, and their environs. *J. Geophys. Res.*, **92**(B9), 8865-8883.

Skolnik, M.I. 1962. *Introduction to radar systems.* New York, McGraw-Hill Book Company.

Skou, N. and F. Sondergaard. 1976. Radioglaciology: a 60 MHz ice sounder system. *Technical University of Denmark. Electromagnetics Institute. Report R 169.*

Ulriksen, C.P.F. 1983. *Application of impulse radar to civil engineering.* Hudson, NH, Geophysical Survey Systems.

Watts, R.D. and D.L. Wright. 1981. Systems for measuring thickness of temperate and polar ice from the ground or from the air. *J. Glaciol.*, **27**(97), 459-469.

Whillans, I.M. and S.J. Johnsen. 1983. Longitudinal variations in glacial flow: theory and test using data from the Byrd Station strain network, Antarctica. *J. Glaciol.*, **29**(101), 78-97.

Whillans, I.M., J. Bolzan, and S. Shabtaie. 1987. Velocity of Ice Streams B and C, Antarctica. *J. Geophys. Res.*, **92**(B9), 8895-8902.

Wright, D.L. and J.F. Prewitt. 1975. Radiating dipole antenna with tapered impedance loading. *IEEE Trans. Antennas Propag.*, **AP-23**(6), 811-814.

Wright, D.L., G.R. Olhoeft, and R.D. Watts. 1984. Ground-penetrating radar studies on Cape Cod. *In Proceedings of the Conference on Surface and Borehole Geophysical Methods in Ground Water Investigations held in San Antonio, Texas, February 7–9, 1984.* U.S. Environmental Protection Agency and National Water Well Association, 666-680.

Wright, D.L., R.D. Watts, and E. Bramsoe. 1986. Single-hole short-pulse borehole radar experiments and a crosshole transponder. *Geol. Surv. Can. Pap.* 85-27, 207-216.

Wright, D.L., J.A. Bradley, and S.M. Hodge. 1989. Use of a new high-speed digital data acquisition system in airborne ice-sounding. *IEEE Trans. Geosci. Remote Sensing*, **27**(5), 561-567.

Wright, D.L., S.M. Hodge, and R.D. Watts. In press. Airborne radar sounding in temperate and polar ice. *In* Fitterman, D.V., *ed. Proceedings of the USGS Airborne EM Workshop held in Denver, Colorado, October 7–9, 1987.*

APPENDIX

SYSTEM SPECIFICATIONS, CONSTRUCTION, AND OPERATION

Table I lists components required for the construction of a pulser of the type used in this work. The theory of operation of the pulser (Fig. 2) is explained in the references, but certain construction and operational details, often learned by trial-and-error, may be helpful to anyone desiring to build and use a similar pulser for ice sounding or other applications.

Three types of transistor have been successfully used in the pulser: 2N2219As, 2N2102s, and MM3009s (in order of increasing rated break-down voltage). Hand selecting sets of transistors for equal break-down voltages is sometimes helpful. Not all transistors of the same type can be used. For example, 2N2102s from International Devices Incorporated have been successful, but those of another manufacturer did not avalanche well. The MM3009s (not the same as 2N3009s) are Motorola transistors and have performed well in avalanche mode. All of the 2N2219As that were tried have been satisfactory. None of these

TABLE I. PULSER-PARTS LIST

Transistors	Q_1-Q_6, 2N2219A or 2N2102 or MM3009
Capacitors	C_1-C_3, 400 pF, 1 kV
Diode	D_1, 1N5711
Resistors	R_1-R_6, 20 kΩ, $\frac{1}{4}$ W
	R_7-R_{12}, 30 Ω
	$R_{13}-R_{18}$, 100 kΩ
	R_{19}, 100 Ω

transistors was designed as an avalanche device, thus it is possible that a manufacturing process change that left a transistor the same in all its rated characteristics would render it unsuitable for use in an avalanche circuit.

When a pulser fails, typically the transistors will no longer stand off the voltage applied to them and are in the "on" state continuously. This can in turn lead to failure of the charging resistors and sometimes the bias and equalizing resistors as well. Power ratings of at least $\frac{1}{4}$ W are advised for the charging resistors. The failure mechanism for the transistors appears to be thermal. In general, the 2N2219s last the longest, the 2N2102s are intermediate, and the MM3009s fail most frequently, consistent with the output power levels. In order to maximize transistor life, heat sinks should be installed on the transistors and the pulser should be operated at less than maximum repetition rate and with the applied voltage below the maximum possible level. The applied voltage must be below the level at which spontaneous break-down occurs, but high enough that the pulser will go into avalanche break-down when trigger pulses are applied. Often, transistor–transistor logic (TTL) devices are sufficient to drive the base of Q_1. If not, a low output impedance buffer stage can be added between a TTL trigger source and Q_1.

A repetition rate of up to 5 kHz is generally safe and, with adequate heat-sinking, continuous operating rates of up to 10 kHz are possible with this design. Above 10 kHz, the peak output power begins to diminish, because the limited output current of the high-voltage power supply is not adequate to recharge fully the capacitors to peak voltage in less than 0.1 ms.

The pulser must always be operated with a load, which can be either an antenna or a resistor in the range of perhaps 50–500 Ω. Capacitors C_1-C_3 must be rated for at least the full applied voltage and should have low loss at frequencies up to 100 MHz. Construction on a copper-clad board is recommended to provide a good ground plane. One-half of the dipole antenna is directly attached to V_{out} and the other half to the pulser ground, which should be isolated from the chassis.

The receiver (Fig. 3) uses wide band-width operational amplifiers with field-effect transistors (FETs) employed as voltage-controlled resistors. Three FETs set the gains of the operational amplifiers and two FETs are in inter-stage resistor divider networks. To achieve a better noise figure, the operational amplifiers are preceded by a low-noise fixed-gain pre-amplifier. Inter-stage high-pass filters are included to prevent feed-through of the amplifier gain (V_g) and resistor-divider shunt (V_s) control voltages and any gain-dependent offset voltages. The components are listed in Table II.

TABLE II. RECEIVER-PARTS LIST

Pre-amplifier	Avantek GPD 401
Operational amplifiers	Comlinear CLC 220
Field-effect transistors	Q_1-Q_5, Siliconix SD210
Resistors	R_1-R_4, 51 Ω
	R_5-R_8, 24 Ω
Capacitors	C_1-C_2, 0.1 μF
	C_3-C_4, 3.3 nF
	C_5-C_6, 470 pF
Inductors	L_1-L_2, 3.3 μH